Drainage Network Extraction from a SAREX'92 RADAR image

ANA LÚCIA BEZERRA CANDEIAS[1]

[1]DPI/INPE–Divisão de Processamento de Imagens / Instituto Nacional de Pesquisas Espacias
Caixa Postal 515
12227– 010 São José dos Campos, SP, Brazil
analucia@dpi.inpe.br

Abstract. The purpose of this paper is to show how to extract the drainage network from the SAREX project RADAR image using Mathematical Morphology tools. The problem is to find a mapping from a grey level image into a binary image that exhibits the drainage. The selected region is from a test site in Acre, SW Amazonia, Brazil. In RADAR images, the drainage network appears with high contrast and well defined shape. Mathematical Morphology is a theory for spatial structure analysis and aims here at analyzing the shape and the forms of the drainage network. This analysis is based on the set and lattice theories. This paper uses the MMach, a Mathematical Morphology Toolbox for the KHOROS system. A comparison between visual analysis and presented method is developed.

Keywords: Image Processing, Mathematical Morphology, Remote Sensing, Radar, Drainage extraction.

1 Introduction

Mathematical Morphology is a theory for spatial structure analysis and aims at analyzing the shape and the forms of objects. It is a powerful tool to extract image information and is based on a mapping study between complete lattices in terms of some families of simple mappings: dilations, erosions, anti–dilations, anti–erosions. These mappings are built combining the elementary mappings through union, intersection and composition operations [Barrera et al. (1995)].

In RADAR images, drainage network appears with high contrast and is usually clearly defined as well as relatively easy to map by visual analysis. Therefore, the drainage network is presented with a well defined spatial structure.

The drainage is significant in helping visual interpretation for nearly every subject, even more so in geology [Trevett (1986)]. Figure 1 (a) shows the selected image from a test site in Acre, SW Amazonia, Brazil.

The drainage network analysis is important to understand the dynamics of annual flooding, to plan development such as location of roads and settlement projects, to estimate the kind of soil and to help the estimation of soil erosion potential.

With simple threshold it is not clearly possible to extract the drainage as shown in Figure 1 (b) because of some parameters like: antenna pattern, speckle and texture patterns.

This paper shows that it is possible to extract the drainage network with Mathematical Morphology mappings and operations. The example selected is from a SAREX'92 RADAR image project.

The objective of SAREX'92 was to acquire a C–band dataset, including simulated satellite data products, to be used for the evaluation of spaceborne C–band SAR data in tropical forest environment [Kux et al. (1993)], [Kux et al. (1995)].

The solution or goal of the drainage network problem is broken heuristically into subgoals, which are achieved by primitive mappings. To achieve the desired goal, the right composition of such mappings is fundamental.

The methodology is implemented using the KHOROS system [Rasure et al. (1990)] and the MMach toolbox [Barrera et al. 1995]. The MMach is composed of a set of primitive mappings and operations. Some of them are defined in section 2.

This paper is divided into four Sections. The next one, Section 2 gives the Mathematical Morphology basic concepts. Section 3 presents the methodology and a comparison between this methodology and the visual analysis extraction. Section 4 presents some conclusions.

2 Mathematical Morphology basic concepts

Mathematical Morphology basic concepts can be seen in [Serra (1982)], [Serra (1988)], [Barrera (1987)], [Haralick et al. (1987)], [Haralick—Shapiro (1991)], [Banon—Barrera (1994)]. For more details about transformation using complete lattices, see [Banon—Barrera (1991)], [Banon—Barrera (1993)]. Mathematical Morphology operators used in Section 3 are defined bellow.

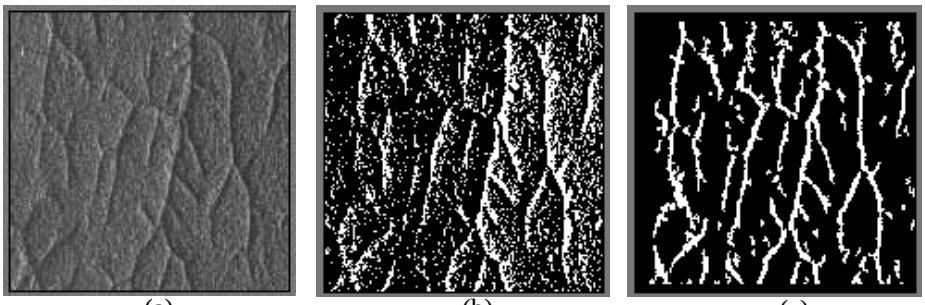

(a) (b) (c)

Figure 1. (a) Original image. (b) Image threshold. (c) MM Binarization.

2.1 Basic image operations and transformations [Barrera et al. (1995)]

Let $\mathbb{Z}$ be the set of integers. Let E be a rectangle of $\mathbb{Z}^2$and let K be an interval $[0, k]$ of $\mathbb{Z}$, with $k > 0$. The collection of functions from E to K will represent the *gray–scale images* of interest. We denote such a collection by K^E and by f, g, f_1 and f_2 generic elements of K^E.

We first recall some useful *local* operations definitions on images. These definitions are based on the structural properties of the interval $[0, k]$ of $\mathbb{Z}$

The *intersection of* f_1 *and* f_2, denoted $f_1 \wedge f_2$, is the function in K^E given by, for any x in E,

$$(f_1 \wedge f_2)(x) = \min\{f_1(x),\ f_2(x)\}, \qquad (1)$$

the *union of* f_1 *and* f_2, denoted $f_1 \vee f_2$, is the function in K^E given by, for any x in E,

$$(f_1 \vee f_2)(x) = \max\{f_1(x),\ f_2(x)\}. \qquad (2)$$

The two binary operations $\wedge$ and $\vee$ from $K^E \times K^E$ to K^E are called, respectively, *intersection* and *union*. Actually, these operations applied to f_1 and f_2 produced, respectively, the infimum and the supremum of f_1 and f_2 with respect to the partial ordering $\leq$ given by

$$f_1 \leq f_2 \Leftrightarrow (f_1(x) \leq f_2(x) \quad (x \in E)).$$

The *complementary* (or *inverse*) *of* f, denoted $\sim f$, is the function in K^E given by, for any x in E,

$$(\sim f)(x) = k - f(x). \qquad (3)$$

The unary operation $\sim$ from K^E to K^E is called *complementary operation* (or *inversion*). This unary operation is both an anti–dilation and an anti–erosion.

The *difference between* f_1 *and* f_2, denoted $f_1 \sim f_2$, is the function in K^E given by, for any x in E,

$$(f_1 \sim f_2)(x) = \begin{cases} f_1(x) - f_2(x) & \text{if } f_2(x) \leq f_1(x) \\ 0 & \text{otherwise.} \end{cases} \qquad (4)$$

The binary operation $\sim$ from $K^E \times K^E$ to K^E is called *difference operation* (or *subtraction*). Actually, we have $f_1 \sim f_2 \leq f_1 \wedge (\sim f_2)$ and we get the equality for *binary images*, that is, for $f_1(E) = f_2(E) = \{0,\ k\}$.

Given a function $f \in K^E$, the unary operation $f \sim \cdot$ is both an anti–dilation and an anti–erosion, and the unary operation $\cdot \sim f$ is both a dilation and an erosion.

The *comparison between* f_1 *and* f_2, denoted $f_1 \leqq f_2$, is the function in K^E given by, for any x in E,

$$(f_1 \leqq f_2)(x) = \begin{cases} k & \text{if } f_1(x) \leq f_2(x) \\ 0 & \text{otherwise.} \end{cases} \qquad (5)$$

The binary operation $\leqq$ from $K^E \times K^E$ to K^E is called *comparison operation*. The unary operations $\cdot \leqq f$ and $f \leqq \cdot$ from K^E to K^E are called *adaptive thresholds with respect to f*. These unary operations are, respectively, an anti–dilation and an erosion.

We now recall the definitions of two important subclasses of dilations and erosions. These definitions are based on the Abelian group property of $(\mathbb{Z}^2, +)$.

Let B be a subset of $\mathbb{Z}^2$, called *structural set* (or, *structural element*). We denote by B_h the *translate of B by* any vector h in $\mathbb{Z}^2$, that is,

$$B_h = \{x + h : x \in B\}.$$

We denote by B^t the *transpose of B*, that is,

$$B^t = \{-x : x \in B\}.$$

We denote by B^c the *complement of B*, that is,

$$B^c = \{x :\ x \notin B\}.$$

The *dilation of f by B* is the function $\delta_B(f)$ in K^E, given by, for any x in E,

$$\delta_B(f)(x) = \max\{f(y) : y \in B^t{}_x \cap E\}; \qquad (6)$$

the *erosion of f by B* is the function $\varepsilon_B(f)$ in K^E, given by, for any x in E,

$$\varepsilon_B(f)(x) = \min\{f(y) : y \in B_x \cap E\}. \qquad (7)$$

In the above expressions, we recall that $\max(\emptyset) = 0$ and $\min(\emptyset) = k$.

The two transformations δ_B and ε_B from K^E to K^E are called, respectively, *dilation* and *erosion by B*.

Let g be an element of K^E, the transformations $\delta_{B,g}$ and $\varepsilon_{B,g}$ from K^E to K^E, given by

$$\delta_{B,g} = \delta_B \wedge g \quad \text{and} \quad \varepsilon_{B,g} = \varepsilon_B \vee g, \quad (8)$$

are called, respectively, *conditional* (or *geodesic*) *dilation* and *erosion* with respect to *B given g*.

The transformations γ_B and ϕ_B from K^E to K^E, given by the following compositions

$$\gamma_B = \delta_B\varepsilon_B \quad \text{and} \quad \phi_B = \varepsilon_B\delta_B, \quad (9)$$

are called, respectively, (*morphological*) *opening* and *closing* with respect to *B*.

Let A and B be two subsets of $\mathbb{Z}^2$ such that $A \subset B$, the two transformations $\lambda_{A,B}$ and $\mu_{A,B}$ from K^E to K^E, given by the following compositions

$$\lambda_{A,B} = \varepsilon_A \wedge \delta^{a}{}_{B^{ct}} \quad \text{and} \quad \mu_{A,B} = \delta_A \vee \varepsilon^{a}{}_{B^{ct}}, \quad (10)$$

are called, respectively, (*morphological*) *sup–generator* and *inf–generator* with respect to *B*.

Let B be a subset of $\mathbb{Z}^2$, the two transformations δ_B^n and ε_B^n from K^E to K^E, given, for $n > 0$, by the following $n-1$ successive compositions

$$\delta_B^n = \delta_B \ldots \delta_B \quad \text{and} \quad \varepsilon_B^n = \varepsilon_B \ldots \varepsilon_B, \quad (11)$$

are called, respectively, *n–dilation* and *n–erosion by B*. Actually, δ_B^n and ε_B^n are, respectively, equivalent to the dilation and erosion by nB, where nB is given by the following $n-1$ successive compositions

$$nB = (B \oplus B) \ldots \oplus B$$

and, for $n = 0$, $nB = \{o\}$.

Let g be an element of K^E, the transformations $\delta_{B,g}^n$ and $\varepsilon_{B,g}^n$ from K^E to K^E, given by the following $n-1$ successive compositions

$$\delta_{B,g}^n = \delta_{B,g} \ldots \delta_{B,g} \text{ and } \varepsilon_{B,g}^n = \varepsilon_{B,g} \ldots \varepsilon_{B,g}, \quad (12)$$

are called, respectively, *n–conditional dilation* and *erosion* with respect to *B given g*.

Let B be a subset of $\mathbb{Z}^2$ and let f be an element of K^E, the transformations $\gamma_{B,f}$ and $\phi_{B,f}$ from K^E to K^E, given by, for any $g \in K^E$,

$$\gamma_{B,f}(g) = \bigvee \{\delta_{B,g}^n(f): n = 1, \ldots\} \quad \text{and}$$
$$\phi_{B,f}(g) = \bigwedge \{\varepsilon_{B,g}^n(f): n = 1, \ldots\}, \quad (13)$$

are called, respectively, *opening* and *closing by reconstruction from the marker f*.

3 Drainage network extraction

Section 2 illustrated some Mathematical Morphology tools. These tools are used in this section to extract the drainage network.

The problem is to find a mapping ψ from a grey level image f into a binary image g that exhibits the drainage. Figure 2 shows an example of this transformation .

The mapping ψ uses the fact that an image can be seen as a 3D mapping (pixel position x, y and its gray level z). The drainage is represented by low gray levels and can be seen by a valley.

To reduce the texture effect, the image is a mean filter using a 3x3 mask (see Figure 3). The methodology is presented in Figure 4. The images shown in this figure are cut out from the original one. filter1, filter2 and filter3 extract the drainage with different structural elements. The box vmsup makes the union among filter1, filter2 and filter3 results.

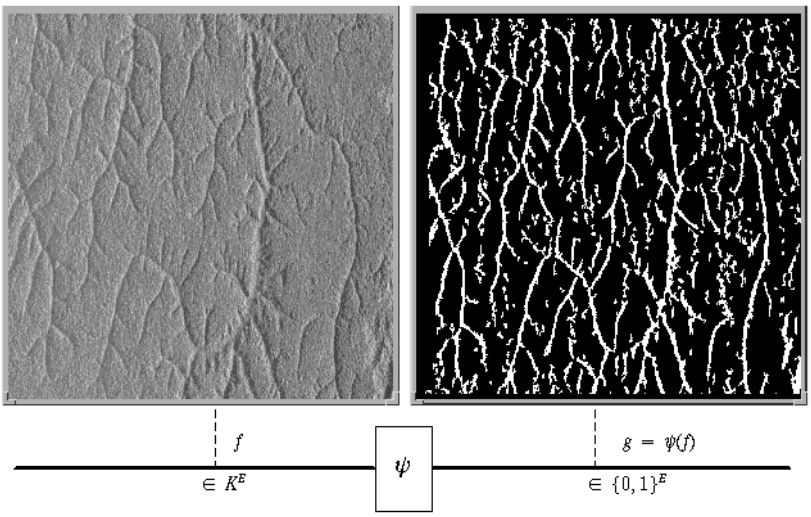

Figure 2. Drainage network extraction.

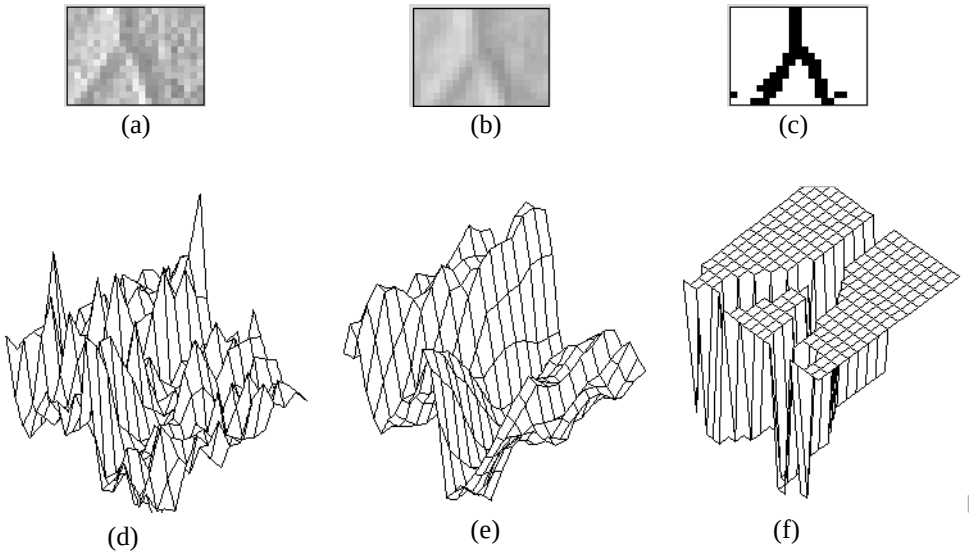

Figure 3. (a) Original image. (b) Low pass filtered image. (c) Binary result of drainage network. (d) 3D mapping of original image. (e) 3D mapping of low pass filtered image. (f) 3D mapping of binary result of drainage network.

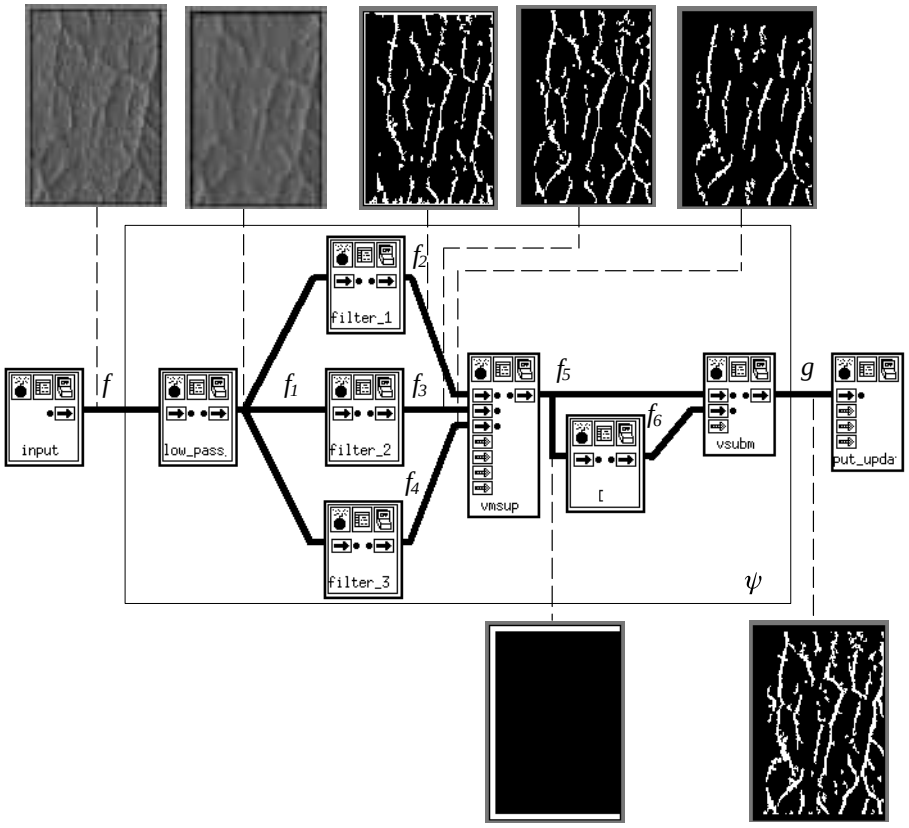

Figure 4. Visual programming to show mapping ψ.

This methodology generates a resulting image with noise represented by left vertical, top and bottom lines with 255 gray levels. This spurious noise is identified by a mask called "[". These lines are suppressed by the box vsubm.

The representation of the structural elements is identified here by binary to decimal coding. Each line is represented by a decimal number. For example B024 is a 3x3 structural element with the origin in the center of the mask. The origin is represented by ".". Then: $B024 = \begin{bmatrix} 0 & 0 & 0 \\ 0 & 1. & 0 \\ 1 & 0 & 0 \end{bmatrix}$ and 8B024 is seven successive compositions of B024. After equation (11) , there is an explanation about it.

Figure 4 presents the methodology in form of visual programming (cantata–KHOROS). Each box of this figure is shown below.

1) **Low pass** filtering to smooth the input image. This step reduces the image texture.

$$f_1 = lp_M(f). \tag{14}$$

Where $lp_M()$ is a mean filter using 3x3 mask M.

2) **filter1** identifies the drainage in the 45^o direction. This identification is based on finding the local minimum by a comparison between two images. For example, let h be an image. The comparison made in equation (15) will generate an h_1 image which selects a local minimum and a homogeneous region of h image :

$$h_1(x) = \begin{cases} k & \text{if } h(x) \leq \varepsilon_B(h(x)) \\ 0 & \text{otherwise.} \end{cases} \tag{15}$$

If there is a lot of texture, h_1 will appear with a lot of noise. If B is larger, then the noise decreases. To identify the drainage in the 45^o direction, the comparison is described as following:

$$g_1 = byte(f_1). \tag{16}$$

Where $byte()$ is cast to byte.

$$g_2 = \varepsilon_{B_1}(g_1). \tag{17}$$

Where $B_1 = 8B024$.

$$g_3 = \varepsilon_{B_2}(g_1) \tag{18}$$

Where $B_2 = B120$.

The comparison between g_1 and g_2 generates a binary result of the drainage with spurious noise .

$$g_4(x) = \begin{cases} k & \text{if } g_1(x) \leq g_2(x) \\ 0 & \text{otherwise.} \end{cases} \tag{19}$$

It can be defined too by:

$$g_4 = (g_1 \leq g_2). \tag{20}$$

Pixels from drainage can be defined by local minimum. If a large structural element B was chosen to find the drainage, the binary image would contain the drainage and less noise. It is possible to identify and suppress part of the present noise in g_4 by applying equations described as following.

First, a comparison between g_1 and g_3 generates a binary result.

$$g_5(x) = \begin{cases} k & \text{if } g_1(x) \leq g_3(x) \\ 0 & \text{otherwise.} \end{cases} \tag{21}$$

$$g_5 = (g_1 \leq g_3). \tag{22}$$

$$g_6 = g_4 - g_5. \tag{23}$$

The equation above reduces some spurious noise. Equation (24) identifies isolated pixels and equation (25) takes away these pixels.

$$g_7 = \lambda_{B_3, B_4}(g_6). \tag{24}$$

Where $B_3 = B020$ and $B_4 = B757$.

$$g_8 = g_6 - g_7. \tag{25}$$

Equation (26) gets g_8 like a marker for image g_4 and reconstructs the drainage network.

$$f_2 = \gamma_{B_5, g_8}(g_4). \tag{26}$$

Where $B_5 = B777$.

3) **filter2** identifies drainage in the 0^o direction. The processing sequence is almost the same as for step 2. The change is only in the structural element of g_2 and g_3, $B_1 = 8B060$ and $B_2 = B030$. The image resulting is f_3.

4) **filter3** identifies drainage in the -45^o direction. The processing sequence is the same as for step 2. The change is only in the structural element of g_2 and g_3, $B_1 = 8B420$ and $B_2 = B021$. The image resulting is f_4.

5) The union (**vmsup**) of filter1, filter2 and filter3 images generates the image f_5 (see Figure 4) .

$$f_5 = f_2 \vee f_3 \vee f_4. \tag{27}$$

6) The box called "**[**" presents the mask. Equation (28) to (32) generates this mask.

$$g_1 = byte(f_5). \tag{28}$$

Where $byte()$ is cast to byte.

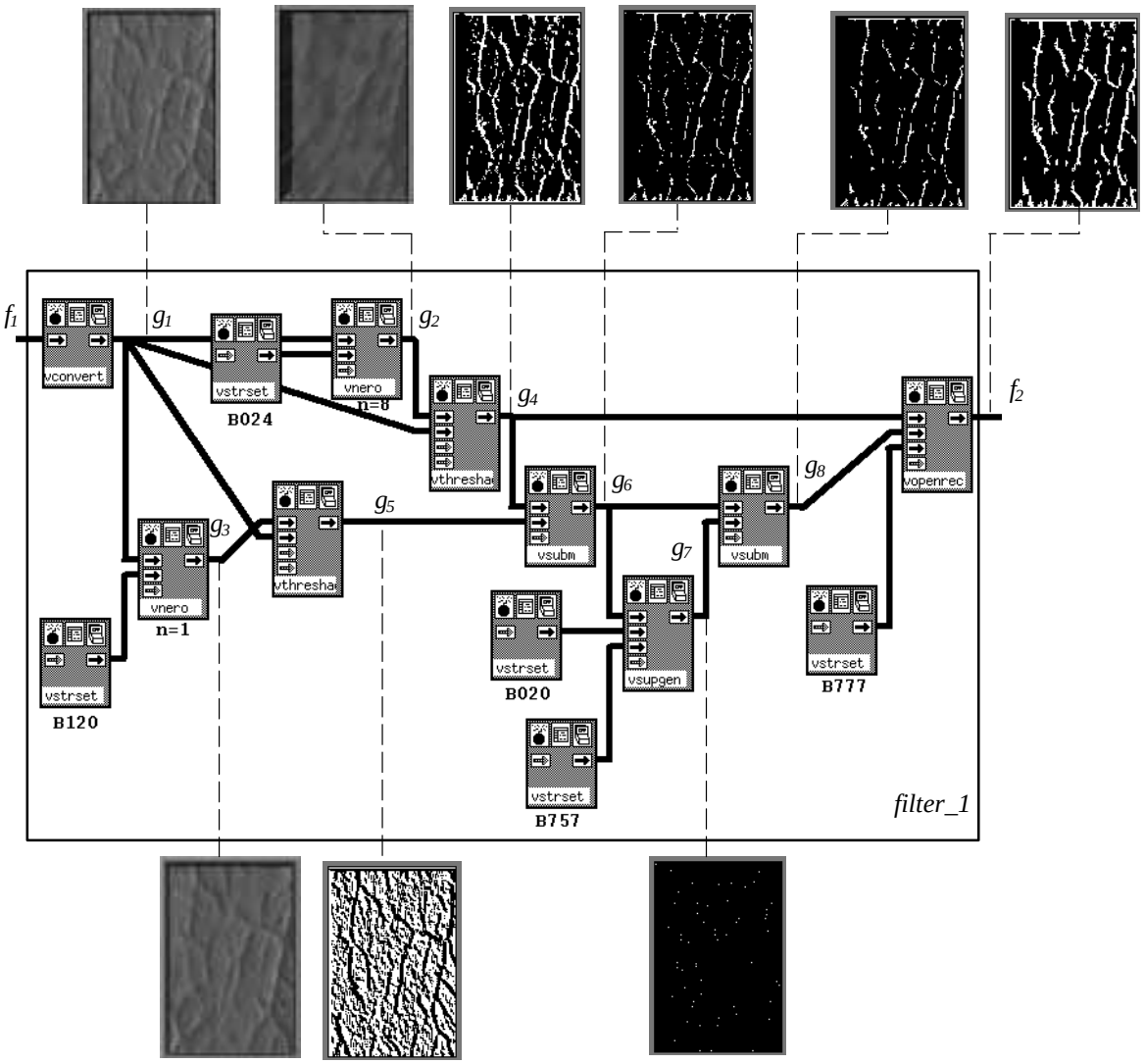

Figure 5. Visual programming of filter_1 box.

Equation (29) generates a black *nxm* image to any *nxm* input image and assigns, automatically, the correct dimension *nxm* to the Cantata visual programming.

$$g_2 = g_1 - g_1. \tag{29}$$

The union of images g_3, g_2 and g_5 generates the mask "[".

$$g_3 = \varepsilon_{B040}(g_2). \tag{30}$$

$$g_4 = \varepsilon_{B400}(g_2). \tag{31}$$

$$g_5 = \varepsilon_{B004}(g_2). \tag{32}$$

$$f_6 = g_3 \vee g_4 \vee g_5. \tag{33}$$

7) The box called "**vsubm**" subtracts the image f_5 from the mask f_6 (see Figure 4). Then the top, bottom and the left side of image f_5 are taken away.

$$g = f_5 - f_6. \tag{34}$$

3.1 Comparison between visual analysis and automatic drainage extraction

In section 3 an automatic drainage extraction was seen. In this section, the automatic extraction is compared with the visual analysis extraction to verify the quality of this mapping. Figure 8 shows a drainage extraction by using the visual analysis (image *x*) and an automatic one (image *y*). Image *y* is defined as following:

$$y = \gamma_{B,X}(\sigma_{B_1 B_2 B_3 B_4}(g)). \tag{35}$$

where $\sigma(g)$ is the g image skeleton defined by Jang and Chin (1990) [Banon—Barrera, 1994] and is included in MMach toolbox. $B = B777$, $B_1 = B032$, $B_2 = B640$, $B_3 = B072$ and $B_4 = B200$.

It is assumed that the white pixels from the automatic extraction image y belong to $\mathcal{A}$ and the white pixels from the visual extraction image x belong to $\mathcal{B}$ and both belong to a set $\mathcal{S}$ (see Fig. 7). The ideal case is when $\mathcal{A} = \mathcal{B}$ and the worst one is when $\mathcal{A} \cap \mathcal{B} = \emptyset$. If an automatic extraction is good $NP(\mathcal{A} \cap \mathcal{B})$ is close to $NP(\mathcal{A} \cup \mathcal{B})$, otherwise, $NP(\mathcal{A} \cap \mathcal{B})$ is low compared with $NP(\mathcal{A} \cup \mathcal{B})$. Where $NP()$ computes the number of elements.

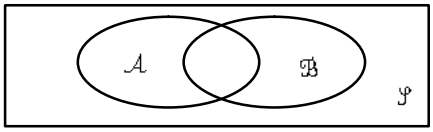

Figure 7. Venn Diagram.

It is supposed that both extraction have some errors. So a distance tolerance is included in $\mathcal{A} \cap \mathcal{B}$. The tolerance is obtained by dilation of x and y by B.

More precisely, the following expressions are introduced [Banon (1996)]:

Error region of type 1 called by exceed error image:

$$e = y - \delta_B(x). \tag{36}$$

Error region of type 2 called by absence error image:

$$f = x - \delta_B(y). \tag{37}$$

Agreement region of type 1 selection:

$$a_2 = y \wedge \delta_B(x) \tag{38}$$

Agreement region of type 2 selection:

$$a_1 = x \wedge \delta_B(y). \tag{39}$$

The next step is to compute the number of pixels, $NP()$ of each region defined in (36) to (39). Let $NP(a)$ be the average of the pixel number of the agreement regions,

$$Np(a) = (Np(a_1) + Np(a_2))/2. \tag{40}$$

The number of pixels percentage in each region is defined by:

a) Let $NP(a)\%$ be the degree of agreement given by:

$$NP(a)\% = NP(a)/T\,. \tag{41}$$

b) Let $NP(e)\%$ be the degree of error of type 1 given by:

$$NP(e)\% = NP(e)/T\,. \tag{42}$$

d) Let $NP(f)\%$ be the degree of error of type 2 given by:

$$NP(f)\% = NP(f)/T\,. \tag{43}$$

Where $T = NP(a) + NP(e) + NP(f)$.

Table 1 shows the result of each percentage of pixels with $B_1 = B777$, $B_2 = 2B_1$ and $B_3 = 3B_1$.

Table 1 – Percentage of pixels

	NP(a)%	*NP(e)%*	NP(f)%
B_1	51	33	16
B_2	73	22	5
B_3	80	17	3

4 Conclusion

Drainage network extraction is an image analysis problem and is significant in helping visual interpretation for nearly every subject that needs remote sensing data, even more so in Geology.

This paper presented a methodology to extract drainage network from a SAREX'92 radar image using Mathematical Morphology tools. The implementation used the KHOROS system and a MMach toolbox.

The methodology developed here was compared with a visual extraction. A distance tolerance was considered through a dilation by B, assuming some errors in automatic drainage extraction as well as in visual extraction. The larger B is, the larger the tolerance is, and more pixels belong to the agreement region. Results would be better in table 1 if the skeleton from the automatic extraction (see Fig. 8 (c)) were prunned. In table 1, the automatic extraction is 80% right with the visual analysis extraction, supposing a tolerance of three pixels.

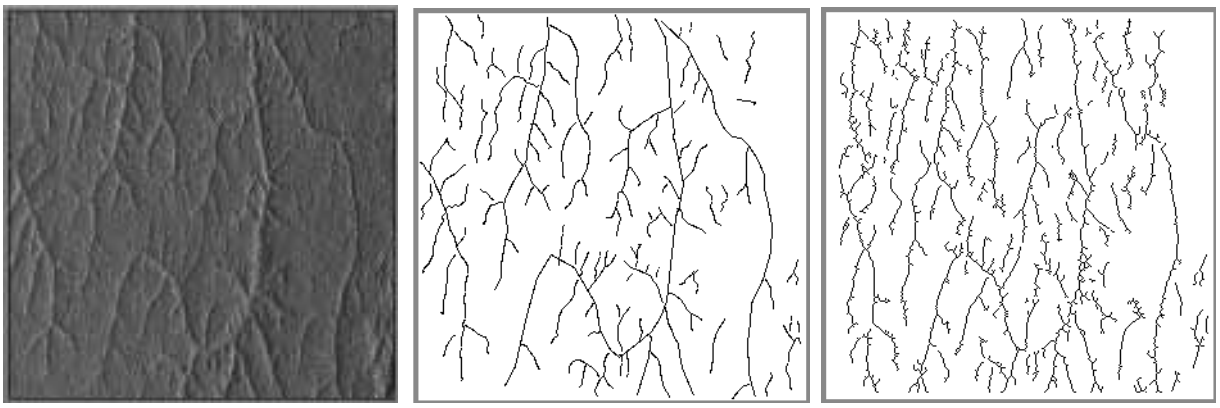

(a) (b) (c)

Figure 8. (a) Original image *f*. (b) Visual extraction, image *x*. (c) Automatic extraction, image *y*.

To use this methodology for other images, some adaptations would be necessary such to smooth the input image and to change the size and direction of the structural element.

Acknowledgment

The author thanks Dr. Gerald J. F. Banon for his suggestions to solve this problem, Dr. Herman Kux for having supplied the image and Marco Aurélio Carvalho for English review.

During the elaboration period of this paper, the author obtained the support of CNPq/ProTeM–CC through AnIMoMat contract 680067/94–9.

Bibliography

B. K. Jang and R. T. Chin, "Analysis of thinning algorithms using Mathematical Morphology". *IEEE Transactions on Pat. Anal. mach. Intel*. (12),6,1990.

G. J. F. Banon, *Personal communication* , ago, 1996.

G. J. F. Banon and J. Barrera, "Minimal representations for translation invariant set mappings by mathematical morphology," *SIAM Journal of Applied Mathematics*, 51, 6(1991):1782–1798.

G. J. F. Banon and J. Barrera, "Decomposition of mappings between complete lattices by Mathematical Morphology. Part I: General lattices," *Signal Processing*, 30(1993):299–327.

G. J. F. Banon and J. Barrera, Bases da Morfologia Matemática para a análise de imagens binárias. *IX Escola de Computação*, Recife, 24 –31, julho, 1994.

H. J. H. Kux, F. J. Ahern and R. W. Pietsch, "Evaluation of radar remote sensing for natural resource management in the tropical rainforests of Acre State, Brazil", Canadian Journal of Remote Sensing, 21, 4(1995):430–440.

H. J. H. Kux, F. J. Ahern, R. K. Raney, R. W. Pietsch, B. Tittley "The contribuition of SAREX'92 (South American RADAR Experiment) Campaign to the evaluation of Natural Resources in Tropical Rainforests: First Results From Test Site Acre, SW–Amazonia, Brazil", In: 16th Canadian Symposium on Remote Sensing, proceedings, Sherbrooke, Quebec, Canada, _(1993):53–58.

J. Barrera, *Uma abordagem unificada para os problemas de Processamento Digital de Imagens: a Morfologia matemática*. Dissertação de mestrado, INPE, São José dos Campos, 1987.

J. Barrera, G. J. F. Banon e R. A. A. Lotufo. A mathematical morphology toolbox for the KHOROS system: specifications for Version 1.2b. *Workshop'95 de Morfologia matemática*, Campinas, mar., 1995. Available at http://www.inpe.br/~banon/URLib2, URLib repository: ime.usp.br/jb/1996/04.03.14.02, 1996.

J. Rasure, D. Argiro, T. Sauer and C. Williams, "Visual Language and Software Development Environment for Image Processing," *International Journal of Imaging Systems and Technology*, 2(1990):183–199.

J. Serra, *Image Analysis and Mathematical Morphology. Volume 1*, Academic Press, London, 1982.

J. Serra, *Image Analysis and Mathematical Morphology. Volume 2: Theoretical Advances*, Academic Press, London, 1988.

J. W. Trevett, "Imaging radar for resource surveys", Chapman and Hall, London, 313p.

R. M. Haralick, S. R. Sternberb and X. Zhuang. Image analysis using mathematical morphology, *IEEE Patern Anal. Machine Intell.*, vol. PAMI–9, 4(1987):532–555.

R. M. Haralick and L. G. Shapiro. Computer and robot vision, vol. 1, New York, Addison Wesley, 1991.